The mycobacterial thioredoxin peroxidase can act as a one-cysteine-peroxiredoxin

Madia Trujillo[*#], PierLuigi Mauri[§#], Louise Benazzi[§], Marcelo Comini[¶], Antonella De Palma[§], Leopold Flohé[‡], Rafael Radi[*], Matthias Stehr[+], Mahavir Singh[+], Fulvio Ursini[‖], and Timo Jaeger[+‡]**

From the [*]Departamento de Bioquímica, Facultad de Medicina, Universidad de la República, Avda. General Flores 2125, UY-11800 Montevideo, Uruguay, [§]Institute for Biomedical Technologies, National Research Council, Via Fratelli Cervi 93, I-20090 Segrate (Milano), Italy, [¶]Centre of Biochemistry, University of Heidelberg, Im Neuenheimer Feld 504, D-69120 Heidelberg, Germany, [‡]MOLISA GmbH, Universitaetsplatz 2, 39106 Magdeburg, Germany, [+]Department of Genome Analysis, German Research Centre for Biotechnology, Mascheroder Weg 1, D-38124 Braunschweig, Germany, and [‖]Department of Biological Chemistry, University of Padova, Viale G. Colombo 3, I-35121 Padova, Italy

Running title: Enzymatic mechanism of mycobacterial TPx.

[#]These authors equally contributed to this work.

[**]To whom correspondence should be addressed: MOLISA GmbH, Molecular Links Sachsen-Anhalt, Universitaetsplatz 2, D-39106 Magdeburg, Germany. Tel.: +49-391-6712463; Fax: +49-391-6718204; E-mail: t.jaeger@molisa.biz.

Thioredoxin peroxidase (TPx) has been reported to dominate the defense against H_2O_2, other hydroperoxides and peroxynitrite at the expense of thioredoxin (Trx) B and C in *Mycobacterium tuberculosis* (*Mt*). By homology, the enzyme has been classified as an atypical 2-C-peroxiredoxin (Prx), with C60 as the "peroxidatic" cysteine (C_P) forming a complex catalytic center with C93 as the "resolving" cysteine (C_R). Site-directed mutagenesis confirms C60 to be C_P and C80 to be catalytically irrelevant, while replacing C93 with serine leads to fast inactivation as seen by conventional activity determination, which is associated with oxidation of C60 to a sulfinic acid derivative. However, in comparative stopped-flow analysis, wt-*Mt*TPx and *Mt*TPx C93S reduce peroxynitrite and react with TrxB and C similarly fast. Reduction of pre-oxidized wt-*Mt*TPx and *Mt*TPx C93S by *Mt*TrxB is demonstrated by monitoring the redox-dependent tryptophan fluorescence of *Mt*TrxB. Furthermore, *Mt*TPx C93S remains stable for 10 min at a SIN-1-generated low flux of peroxynitrite and excess *Mt*TrxB in a dihydrorhodamine oxidation model. LC-MS/MS analysis reveals disulfide bridges between C60 and C93 and between C60 and C80 in oxidized wt-*Mt*TPx. Reaction of pre-oxidized wt-*Mt*TPx and *Mt*TPx C93S with *Mt*TrxB C34S or *Mt*TrxC C40S yields dead-end intermediates in which the Trx mutants are preferentially linked *via* disulfide bonds to C60 and never to C93 of the TPx.

It is concluded that neither C80 nor C93 are required for the catalytic cycle of the peroxidase. Instead, *Mt*TPx can react as a 1-C-Prx with C60 being the site of attack for both the oxidizing and the reducing substrate. The role of C93 is likely to conserve the oxidation equivalents of the sulfenic acid state of C_P as a disulfide bond to prevent over-oxidation of C60 under a restricted supply of reducing substrate.

The peroxide metabolism of *M. tuberculosis* is intriguing in several respects:

i) Like other actinomycetes *M. tuberculosis* lacks glutathione, and, consequently, the glutathione peroxidases that dominate the antioxidant defense of its mammalian hosts (1). *ii)* The pathogen's H_2O_2 metabolism has long been recognised to depend on a heme-containing

catalase/peroxidase, since experimental *KatG*$^{-1}$ strains devoid of this heme protein were found to be avirulent (2). *iii*) Clinical isolates lacking the catalase were however virulent and proved to be resistant against the first line tuberculostatic INH, because the enzyme is evidently required to activate this drug (3). *iv*) The survival and virulence of such strains is attributed to a 2-C peroxiredoxin-type peroxidase, AhpC, because it was often found elevated in catalase-deficient clinical isolates (2). *v*) The most common AhpC reductant of bacteria, the disulfide reductase AhpF, is however deleted in *M. tuberculosis* and the rudimentary alkyl hydroperoxide reductase system appears not to respond to oxidative stress like in enterobacteria (4), since a functional *oxyR* is equally missing (5). *vi*) Instead, *Mt*AhpC can be reduced by AhpD, a CXXC motif-containing enzyme that can be recycled by protein-bound lipoic acid of the α-keto acid dehydrogenase complex (6) or by one of the mycobacterial thioredoxins, *Mt*TrxC (7). *vii*) Mycobacteria contain two more peroxiredoxins, the 1-C-Prx AhpE, whose function still remains elusive (8), and the "thiol peroxidase" *Mt*TPx, which proved to be a thioredoxin peroxidase (7).

*Mt*TPx, which is addressed here, has recently been characterized as the most effective peroxidase of *M. tuberculosis* in terms of rate constants for the reaction with hydroperoxides and peroxynitrite. It reduces a broad spectrum of hydroperoxides including H_2O_2 and its reduced state is specifically regenerated by two of the mycobacterial thioredoxins, *Mt*TrxB and *Mt*TrxC. According to available proteomes of *M. tuberculosis*, *Mt*TPx is regularly more abundant than the better known antioxidant enzymes catalase/peroxidase and AhpC and may therefore be considered to be the dominant antioxidant device that guarantees the pathogen's survival in the oxidant environment of the host's phagocytes. The enzyme has a limited similarity with human Prxs, the most similar one being PrxII with only 21 % identities. This dissimilarity to mammalian sequences as well as the putative functional importance underscores the potential use of *Mt*TPx as a drug target.

By sequence, *Mt*TPx is classified as an atypical 2-cysteine peroxiredoxin (2-C-Prx). It is closely related to a variety of "thiol peroxidases", of which the thioredoxin peroxidase of *Escherichia coli* has been most extensively investigated in terms of structure (9) and functional aspects (10). The catalytic mechanism common to all peroxiredoxins consists in the oxidation of a highly reactive 'peroxidatic' cysteine (C_P) to a sulfenic acid derivative, which is followed by a direct or indirect reduction by a thiol substrate (11,12). As was first shown for the tryparedoxin peroxidase of *Leishmania donovani* (13), the activation of C_P is achieved by the positive charge of a neighboring arginine residue and hydrogen bonding with a threonine or, less commonly, a serine residue, which forces the active site cysteine into the thiolate form that readily reacts with any kind of ROOH (14). The reduction of the resulting sulfenic acid differs between different types of Prxs. In the case of the typical 2-C-Prxs, the primary reductant is a cysteine conserved near the C-terminus ('C_R' for resolving cysteine) that forms a disulfide bridge with C_P, which then reacts with the reducing substrate, typically a protein containing a CXXC motif such as thioredoxin, tryparedoxin or AhpF (14,15). However, since C_R is sterically out of reach for C_P within the same protein subunit, the disulfide is formed between two inversely oriented subunits. During this process C_P is delocalized in a way that it is no longer accessible to the reducing substrate. The catalysis would therefore be arrested in the oxidized form, if the reducing substrate could not "resolve" this block by attacking the sulphur of the distally conserved cysteine, which thus becomes the C_R. In 1-C-Prxs the C-terminal cysteine is not conserved and the reducing thiol substrate has to react directly with the oxidized C_P. In the atypical 2-C-Prxs the C_R typical of the 2-C-Prxs is also missing but another cysteine is presumed to substitute for C_R in a way that it forms an intra-subunit disulfide bridge that is the prerequisite to terminate the catalytic cycle (9).

The recently resolved x-ray structures of *Mt*TPx (pdb-id 1XVQ), of the molecular mutant *Mt*TPx C60S (pdb-id 1Y25, (16)) and of the related peroxiredoxins of *Haemophilus influenzae* (pdb-id 1Q98), *E. coli* (pdb-id 1QXH, (9)) and *Salmonella pneumoniae* (pdb-id 1PSQ) reveal that C60 in *Mt*TPx builds the center of the catalytic triad typical of Prxs, which here is composed of C60, T57 and R130. C60 thus should be the peroxidatic cysteine, while C93 is homologous to the presumed C_R of related atypical 2-C-Prxs and the 3rd cysteine in *Mt*TPx, C80, remains of questionable functional relevance. The x-ray structures, however, did not provide unambiguous

evidence for any obligatory involvement of C93 in the catalysis. In fact, the Cα distance between S60 (corresponding to C60) and C93 in *Mt*TPx C60S appeared too large to allow a disulfide formation without major rearrangements (Fig. 1), the expected C60 – C93 disulfide bond is not clearly visible in the structure of oxidized *Mt*TPx (pdb-id 1XVQ) either, and the substantial residual activity of *Ec*TPx C95S that has more recently been reported by Baker and Poole (10) sheds further doubt on the hypothesis that the distal conserved cysteine of the atypical 2-C-Prxs is always functionally equivalent to the resolving cysteine of typical 2-C-Prxs.

Here we present compelling evidence for a novel variation of Prx catalysis. The catalytic mechanism of *Mt*TPx does not necessarily involve the presumed C_R but rather corresponds to that of a 1-C-Prx. The cysteine homologous to C_R, however, prevents inactivation of the enzyme by hydroperoxides under limited supply of reductants by saving the oxidation equivalents in a readily reversible oxidation state.

EXPERIMENTAL PROCEDURES

Preparation of proteins – *Mt*TPx, *Mt*TrxB and *Mt*TrxC were heterologously expressed as His-tagged proteins in *E. coli* as described by Jaeger *et al.* (7). Mutations C60S, C80S and C93S were introduced into *Mt*TPx by site-directed mutagenesis PCR (17) using the TPx gene cloned into pET22b(+) as template (7). For the C60S mutation the following mismatched primers were used: 5´-caccggtgtccgcgacgagtg-3´ (forward) and 5´-cactcgtcgcggacaccggtg-3´ (backward), the C80S mutation was introduced with the mismatched primers 5´-ccgtgctgtccgtctcgaagg-3´ (forward) and 5´-ccttcgagacggacagcacgg-3´ (backward), and that of C93S mutation with the mismatched primers 5´-gaagcgcttctccggcgccgag-3´ (forward) and 5´-ctcggcgccggagaagcgcttc-3´ (backward). The triplets coding for the mutations are underlined. Each mutation was introduced with the forward mismatched primer in combination with the pET22b(+) T7 terminator primer (5´-gctagttattgctcagcgg-3´) and the backward mismatched primer in combination with the pET22b(+) T7 promoter primer (5´-taatacgactcactataggg-3´). Reaction mixtures contained 10 - 40 ng of template DNA, 125 ng of each primer, 20 µM dNTPs and 1 µl PfuTurbo Polymerase (Stratagene, La Jolla, USA). 30 Cycles of 95 °C for 30 s, 50 °C for 60 s and 72 °C for 1 min were carried out in a Tpersonal Cycler (Biometra, Goettingen, Germany) followed by 72 °C for 10 min. Both resulting PCR products that carried the mutation were cut from a 1 % agarose gel and purified with the QIAquick Gel Extraction Kit (Qiagen, Hilden, Germany). Similarly, the mutants of *Mt*TrxB and C were obtained by mutating the distal cysteine, 34^2 or 40, respectively, of the CXXC motif to serine. Briefly, a first round of PCR (30 cycles at 95 °C for 1 min, 50 °C for 1 min and 72 °C for 2 min) using Proof Start DNA Polymerase (Qiagen) was performed with the following primer pairs: Fo T7-promoter (5'-TTAATACGACTCACTATAGG-3') / Re *Mt*TrxB C34S (5'-GCGAACGCGCGGCTCGGGCCGCA-3') or Re T7-terminator (5'-GCTAGTTATTGCTCAGCGGT-3') / Fo *Mt*TrxB C34S (5'-TGCGGCCCGAGCCGCGCGTTCGC-3') for *Mt*TrxB, and Fo T7-promoter / Re *Mt*TrxC C40S (5'-CTACCATCTTGCTAGGTCCACAC-3') or Re T7-terminator / Fo *Mt*TrxC C40S (5'-GTGTGGACCTAGCAAGATGGTAG-3') for *Mt*TrxC. Plasmids harbouring wild-type genes of *Mt*TrxB or *Mt*TrxC, and engineered to contain a C- or N-terminal His-tag were used as DNA templates (7). The relocation of mutated genes was carried out in a PCR reaction that included both purified overlapping PCR products in combination with the T7 promoter and terminator primer. The purified PCR product was digested with *Nde*I and *Hind*III, ligated into the pET22b(+) vector (Merck Biosciences, Bad Soden, Germany) and subsequently transformed into *E. coli* BL21 (DE3) (TPx mutants) or *E. coli* Tuner (DE3) (Trx mutants), respectively. The DNA sequence was confirmed by DNA sequencing. The mutant proteins were expressed, purified as described (7) and checked for identity by MS/MS analysis.

Kinetic measurements – Conventional activity determinations of *Mt*TPx and derived mutants were performed by means of a coupled test that measures thioredoxin-mediated NADPH consumption by thioredoxin reductase as described by Jaeger *et al.* (7). Pre-incubation conditions were 10 µM thioredoxin reductase, 10 µM thioredoxin B or C, 5 µM *Mt*TPx, 450 µM NADPH, 1 mM EDTA in 50 mM Hepes buffer of pH 7.4 at 25 °C.

The reaction was started with 73 μM t-bOOH (final concentration) and monitored continuously.

Direct stopped-flow measurement of peroxynitrite reduction by *Mt*TPx was performed as follows: Peroxynitrite was freshly synthesized in a quenched-flow reactor from sodium nitrite and hydrogen peroxide (H_2O_2) under acidic conditions and quantified as described previously (18). Stock solutions of peroxynitrite were treated with granular manganese dioxide to eliminate H_2O_2 remaining from the synthesis. Nitrite content in samples of peroxynitrite was typically < 30 % of the peroxynitrite concentration. *Mt*TPx (either wild-type or mutants) and *Mt*TrxC or B were reduced overnight by the addition of a >10-fold excess dithiothreitol (DTT). Excess reductant was removed immediately before use by passing the proteins through a high pressure liquid chromatography-connected Hitrap column (Amersham Biosciences) with UV-visible detection at 280 nm and collected manually in rubber-capped tubes, which were subsequently bubbled with argon at 4 ºC. Total thiol content was determined by Ellmann's reagent to exclude the presence of any relevant residual DTT. The extensively degassed elution buffer was 100 mM sodium phosphate, pH 7, plus 0.1 mM DTPA (diethylenetriamine-pentaacetic acid). The reduction of peroxynitrite by reduced *Mt*TPx (either wild-type or the mutants C60S, C80S or C93S, respectively) was then studied at pH 7.4 and 25 °C in a stopped-flow spectrophotometer (SX-17MV, Applied Photophysics) with a mixing time of less than 2 ms, monitoring peroxynitrite decomposition at 310 nm with or without pre-reduced enzyme at concentrations indicated (19). For the determinations of initial rates of peroxynitrite decomposition, 200 absorbance points were acquired during the first 20 ms of the reaction, and 200 further points were acquired until more than 90 % peroxynitrite had decomposed (0.02 – 20 s). Computer-assisted simulations were performed using Gepasi software (20).

The reduction of peroxynitrite-oxidized *Mt*TPx or its mutants by its natural reductants, i.e. *Mt*TrxB or *Mt*TrxC, was evaluated by monitoring the peroxynitrite decomposition rate at a low *Mt*TPx concentration and its acceleration by *Mt*TrxC or *Mt*TrxB. Precisely, 1.1 μM pre-reduced *Mt*TPx was reacted with 5 μM peroxynitrite to yield a fast initial peroxynitrite reduction followed by the slope typical of spontaneous peroxynitrite decomposition. The slope thus obtained provides the base line to be compared to that observed upon addition of pre-reduced *Mt*TrxB or *Mt*TrxC (33 μM), which by themselves only marginally affect the peroxynitrite decay. The experimental results were then compared to curves calculated by means of known (7) or estimated rate constants.

Alternatively, rates of reduction of *Mt*TPx (or mutants) by TrxB were measured directly taking advantage of redox-dependent fluorescence changes of *Mt*TrxB. The reaction of 2.25 μM *Mt*TrxB, pre-reduced by DTT, with excess *Mt*TPx (or mutants; 15 – 40 μM) was analyzed by stopped-flow technique monitoring the tryptophan fluorescence of *Mt*TrxB at $\lambda > 335$ nm and an excitation wavelength of $\lambda = 280$ nm.

Qualitatively, the reaction of *Mt*TrxB with *Mt*TPx (and molecular mutants) was investigated by monitoring the oxidation of dihydrorhodamine (DHR) by a low flux of peroxynitrite (~0.7 μM/min) generated by SIN-1 (3-morpholinosydnonimine hydrochloride) as follows: 120 μM DHR was exposed to 50 μM SIN-1 yielding a constant oxidation rate of 0.28 μM/min, as is monitored at 500 nm ($\varepsilon = 78{,}800$). The influence of *Mt*TrxB, mutants, *Mt*TPx and combinations thereof on slope and/or lag phase is then taken as a semi-quantitative measure of interference with the oxidation process (19).

LC-ESI-MS/MS analysis of intermediates of the catalytic cycle

Protein reduction and oxidation – If not stated differently, each protein was reduced for 80 min at 37 °C with 50 mM DTT in 50 mM phosphate buffer, pH 7.5. Following removal of the reductant by buffer exchange (gel-filtration on a Bio-Spin 6 columns, twice), TPx 25 μM was mixed in different experiments with 100 μM hydrogen peroxide or 150 μM TrxB. The sequence of additions and incubation times are reported for specific experiments under Results. The reaction was stopped by adjusting the sample to pH 2 by HCl.

Enzymatic digestions – Pepsin was added at an enzyme substrate ratio of 1:100 (w/w) in 100 mM ammonium acetate, pH 2.5. After 3 h incubation at RT, the reaction was stopped by cooling on ice. Trypsin was added at an enzyme substrate ratio of 1:10 (w/w) in 100 mM ammonium bicarbonate, pH 8. After overnight incubation at 37 °C the pH was adjusted to 2 with trifluoroacetic acid to stop

the reaction. Ten µl of the peptide mixtures were applied to LC-ESI-MS/MS.

LC-ESI-MS/MS Analysis of Peptides – For liquid chromatography / mass spectrometry a Surveyor MS HPLC pump equipped with a MicroAS autosampler (loop 20 µl) was coupled to a LTQ ion trap mass spectrometer by an electrospray interface (ThermoElectron, Milan, Italy). An ACE C18 column (1 ×150 mm, 5 µm, ACT, Aberdeen, Scotland) with an acetonitrile gradient was used (eluent A: 0.1% formic acid in water; eluent B: 0.1 % formic acid in acetonitrile) at a flow rate of 50 µl/min. The gradient profile was 5 % B for 4 min followed by 5 to 50 % B within 40 min.

For mass spectrometry, the heated capillary was held at 180 °C and voltage at 38 V. Spray voltage was 5.2 kV. Spectra were acquired in positive mode (in the range 400 – 2000 *m/z*) using dynamic exclusion for MS/MS analysis (relative collision energy of 35 %, repeat count 3).

Data handling of mass spectra – Computer analysis of peptide MS/MS spectra was performed using Bioworks 3.1, based on SEQUEST algorithm (University of Washington, USA, licensed to ThermoFinnigan Corp.). For the peptic peptide mixture the 'no enzyme' option was used due to the limited specificity of pepsin cleavage. As confidence of peptide identification the minimum values of Xcorr were greater than 1.5, 2.0, and 2.5 for single, double and triple charge ions, respectively.

Identification of disulfides was carried out as follows: first the most frequent cysteine-containing peptides obtained by pepsin digestion were identified in both, TPx and Trx. Then these peptides were used for manual calculation of possible peptides linked by disulfide bridges. The minimum consecutive multi-charge ions of a possible "hybrid peptide" were 3. When possible, manual evaluation of related MS/MS spectra were performed to obtain partial amino acid sequences of one or both peptides.

RESULTS

Apparent activity of molecular mutants in conventional test – To define the catalytic role of each of the three cysteines in *Mt*TPx, the molecular mutants C60S, C80S and C93S were first investigated for catalytic efficiency by means of the conventional coupled test system that mimics the enzyme's physiological context: NADPH consumption for hydroperoxide reduction via thioredoxin reductase, *Mt*TrxC and *Mt*TPx. As is evident from Fig. 2 *Mt*TPx C60S is absolutely inactive, while *Mt*TPx C80S is indistinguishable from the wild-type enzyme. The first finding complies with the expectation that C60 is the C_P, the second observation rules out any substantial role of C80 in the catalysis. At first glance the relevance of C93 to catalysis is corroborated by a marginal residual activity of *Mt*TPx C93S. A closer inspection of the trace, however, discloses that for a few seconds a discrete residual activity is retained in *Mt*TPx C93S, while thereafter NADPH consumption approaches that of the negative control. This finding points rather to a fast inactivation than to an abrogation of catalytic efficacy itself.

Stopped-flow analysis of MtTPx oxidation by peroxynitrite – In a first set of experiments, the oxidation of wt-*Mt*TPx and *Mt*TPx mutants by peroxynitrite was measured directly in the millisecond range by monitoring the absorption at $\lambda = 310$, which is characteristic of peroxynitrite. For this purpose the enzyme samples were reduced by DTT and freed of reductant by gel filtration. Their total thiol content was determined to range between 2.6 and 3.4 thiol groups per subunit of protein, which is consistent with the absence of relevant amounts of low molecular thiols. Any traces of undetected residual DTT in this range of concentrations would not have affected the measurements, since its second order rate constant with peroxynitrite is only 1100 $M^{-1}s^{-1}$ (data not shown). In the presence of 40 µM wild-type enzyme, peroxynitrite (18 µM) decays very rapidly, in agreement with the fast second order rate constant (k_1'=1.5 x 10^7 $M^{-1}s^{-1}$ at pH 7.4 and 25 ºC) that was previously reported for peroxynitrite-dependent *Mt*TPx oxidation (7). The reaction is so fast that an important fraction of peroxynitrite (~ 50 %) already decayed during the first 2 ms, ***i. e.*** the mixing-time of the apparatus (Fig. 3). With *Mt*TPx C60S (46 µM) the rate of peroxynitrite decay is practically the same as in the absence of enzyme, confirming that C60 is responsible for the fast peroxynitrite reduction, i.e. C60 is C_P. *Mt*TPx C80S and *Mt*TPx C93S also reacts very fast with peroxynitrite. The rate constant for *Mt*TPx C93S (2 x 10^6 $M^{-1}s^{-1}$) is, in fact, close to that established previously for the wild-type enzyme (1.5 x 10^7 M^{-}

$^{1}s^{-1}$). In view of the pronounced instability of *Mt*TPx C93S under oxidizing conditions the difference is likely explained by an overestimation of the native enzyme. In essence, therefore, the results are hardly compatible with an essential involvement of C93 (or C80) in the oxidative part of the catalytic process.

Reduction of oxidized MtTPx by its natural substrates – As C93 is, by analogy, suspected to be the resolving cysteine, its replacement by serine might selectively affect the interaction with the reducing substrate. The limiting apparent rate constant k_2' for the reduction of oxidized *Mt*TPx by *Mt*TrxB or C had therefore to be analyzed in order to demonstrate if *Mt*TPx C93S can also act as a peroxynitrite reductase when using its natural reductants. This task, however, afforded a control model for which the relevant rate constants had previously been established or were accessible. Therefore, peroxynitrite decomposition in the presence of wt-*Mt*TPx, *Mt*TrxC and combinations thereof was analyzed to evaluate how the system behaves, if the peroxynitrite-oxidized enzyme is being recycled by its reductant. The addition of pre-reduced *Mt*TPx (1.1 μM) to peroxynitrite (5.5 μM) causes a fast initial peroxynitrite-decomposition. After consumption of the under-stoichiometric amount of enzyme, peroxynitrite decays at the rate of spontaneous decomposition (Fig. 4A). The addition of pre-reduced *Mt*TrxC (33 μM) alone, which is also a thiol-containing protein, causes a modest increase in the peroxynitrite decomposition rate (from 0.26 s^{-1} to 0.59 s^{-1}), from which a second order rate constant for the reaction between peroxynitrite and *Mt*TrxC of 1 x 10^4 $M^{-1}s^{-1}$ at pH 7.4 and 25 ºC is estimated. However, in the presence of both *Mt*TPx (1.1 μM) and pre-reduced *Mt*TrxC (33 μM), peroxynitrite decomposition increases substantially, clearly revealing the regeneration of reduced *Mt*TPx by the thioredoxin. In fact, computer-assisted simulations of the reactions according to equations (1) - (4) with the established rate constants perfectly match with the experimental data (Fig. 4B).

$ONOOH \rightarrow NO_3^-$
$k = 0.26\ s^{-1}$ (21) (Eq. 1)
$_{red}$*Mt*TPx + $ONOOH \rightarrow$ $_{ox}$*Mt*TPx + NO_2^-
$k_1' = 1.5 \times 10^7\ M^{-1}s^{-1}$ (7) (Eq. 2)
$_{red}$*Mt*TrxC + $ONOOH \rightarrow$ $_{ox}$*Mt*TrxC + NO_2^-
$k_2' = 1 \times 10^4\ M^{-1}s^{-1}$ (this work) (Eq. 3)
$_{ox}$*Mt*TPx + $_{red}$*Mt*TrxC $\rightarrow$ $_{red}$*Mt*TPx + $_{ox}$*Mt*TrxC
$k_2' = 5.8 \times 10^4\ M^{-1}s^{-1}$ (7) (Eq. 4)

The same kind of experiment was then performed with the mutated forms of *Mt*TPx to unravel the role of C93 (and C60 or C80) in the reductive part of the catalytic cycle. As is shown in Fig. 4C, in the presence of both *Mt*TPx C60S (1.1 μM) and *Mt*TrxC (33 μM) peroxynitrite declined at the same rate as in the presence of *Mt*TrxC alone, which is expected, since *Mt*TPx C60S lacks the peroxidatic cysteine. Surprisingly, however, *Mt*TPx C93S (1.1 μM) in the presence of *Mt*TrxC (33 μM) has the same effect on the peroxynitrite decomposition rate as the wild-type enzyme (Fig. 4A) indicating that it is equally able to sustain the entire catalytic cycle. The experiment was repeated with the second natural reductant of *Mt*TPx, *Mt*TrxB. Again, the C93S mutant accelerated the rate of peroxynitrite reduction by the thioredoxin (Fig. 4D). These observations strongly suggest that C93 is not required to resolve the oxidized state of the enzyme.

For final proof of a reduction of oxidized *Mt*TPx without the aid of C93, i. e. without the necessity to first form a disulfide bridge between C60 and C93, the decline of tryptophan fluorescence of *Mt*TrxB upon oxidation with *Mt*TPx was measured by the stopped-flow technique. For this purpose *Mt*TrxB was reduced by DTT, freed of reductant and then reacted with excess oxidized *Mt*TPx (15 – 40 μM). Despite an unfavorable signal to noise ratio, the decline of fluorescence upon oxidation of *Mt*TrxB could reliably be analyzed (Fig. 5A). When plotting the k_{2obs} against the *Mt*TPx concentrations, a k_2' for the reaction of reduced TrxB with wt-*Mt*TPx was calculated (8.2 x 10^3 $M^{-1}s^{-1}$) that is lower than the one previously obtained by steady-state kinetics by a factor of 5, but which is nevertheless indicative of an efficient and specific reaction taking into account the known tendency of peroxiredoxins to loose activity if kept under oxidizing conditions. More importantly, *Mt*TPx C93S turned out to be at least equally efficient as an oxidant of TrxB (k_2' = 1.1 x 10^4 $M^{-1}s^{-1}$; Fig. 5B), while the mutant lacking C_P (C60S) only marginally affected the fluorescence of the Trx.

Dispensability of C93 at "physiological" fluxes of peroxynitrite – Taken together, the results

reported so far clearly indicate that the presumed C_R is dispensable for sustaining the catalytic cycle of *Mt*TPx, but evidently prevents oxidative inactivation of the enzyme when analyzed at high peroxide concentrations, as are inevitably used for conventional activity determinations. In order to get an idea of the physiological relevance of this protective role of C93, we tested the activity of *Mt*TPx C93S in a model system that allows to monitor the prevention of oxidative damage exerted by a low flux of peroxynitrite, as it may be expected under *in vivo* conditions.

When dihydrorhodamine (DHR) is exposed to SIN-1, it is oxidized by peroxynitrite-derived radicals to rhodamine in a process than can be followed at 500 nm. Under the conditions chosen, a constant DHR oxidation rate of 0.28 µM/min (Fig. 6, shown in black) is obtained after a lag phase of 10 – 15 min. At an estimated oxidation yield of 40 %, peroxynitrite fluxes can be calculated to amount to 0.7 µM min^{-1}. When 1.3 µM *Mt*TPx (wild type, C60S or C93S), which had not been pre-reduced, are added once the lag phase is terminated (15 minutes after the addition of SIN-1), DHR oxidation by SIN-1 is not significantly affected. Pre-reduced *Mt*TrxB (6.7 µM), which at the concentrations chosen should only slowly reduce peroxynitrite, slows down the rate of DHR oxidation to 0.14 µM/min, probably by competing for peroxynitrite-derived radicals (Fig. 6, blue line). In the presence of pre-reduced *Mt*TrxB (6.7 µM), however, wt-*Mt*TPx as well as *Mt*TPx C93S (each at 1.3 µM, shown in red and green, respectively) completely suppresses peroxynitrite-dependent DHR oxidation for almost 10 minutes, which roughly corresponds to the calculated time required for the total consumption of the Trx at given peroxynitrite fluxes. Expectedly, DHR oxidation is thereafter resumed at almost the same rate as in the absence of proteins. *Mt*TPx C60S, as an inactive control, did not interfere at all with DHR oxidation (not shown). The results first of all confirm that *Mt*TPx C93S is fully active as a Trx-dependent peroxidase and that it remains active despite exposure to peroxynitrite, as long as it is continuously reduced by excess of its natural substrate. C93 thus proves to be not only dispensable for activity of *Mt*TPx but does not appear to be absolutely required for its stability either.

Mass spectrometric analysis of observed phenomena – In order to unravel which of the three cysteines of *Mt*TPx can react with each other or with substrates, wt-*Mt*TPx or *Mt*TPx C93S were reacted with oxidizing and reducing substrates and analyzed by LC-MS/MS for revealing fragments, as described below and compiled in Table 1. Pepsin treatment of reaction products was preferentially applied, as the low pH during peptic digestion reliably prevents re-arrangements of disulfide bonds (22), although data analysis is often tedious, due to extensive degradation and poor specificity of pepsin. Complementary analyses had therefore to be performed after tryptic digestion, although the results obtained this way may be compromised by thiol/disulfide exchange due to the required alkaline pH. For identification of the site of preferred attack of the TPx by Trx, the molecular mutants of *Mt*TrxB $C34S^2$ and *Mt*TrxC C40S were used, which have the surface-exposed, reacting cysteines of their CGPC motifs preserved, but the co-reacting cysteines mutated to serine. Although much less reactive than wt-Trxs, these mutants can be expected to target their reaction partners identically in principle but to remain covalently bound to them *via* disulfide bonds (23).

When wt-*Mt*TPx was investigated by LC-ESI-MS/MS immediately after reduction by DTT, expectedly no disulfide-containing fragments were obtained if the protein was cleaved under acidic conditions by pepsin, while each of the three cysteines of the protein were represented in more than one peptic fragment (data not shown). Upon re-oxidation, a fragment of 4105.7 *m/z* was isolated from the peptic digest that contained the sequence of *Mt*TPx 49–66, as verified by MS/MS sequencing, bound to either *Mt*TPx 80–99 or 90–109 isobaric peptides (Table 1, *i*). A second fragment (*m/z* 3261.7) was found composed of *Mt*TPx 53–63 and *Mt*TPx 90–109, thus verifying the formation of the anticipated bond between C60 and C93 (Fig. 7).

When *Mt*TPx C93S was oxidized with H_2O_2 and then reacted with excess wt-TrxB (Table 1, *ii*) a fragment suggestive of a disulfide bond within the TPx mutant could no longer be detected. Instead, oxidized TrxB was clearly identified, underscoring that the mutant TPx is enzymatically active. Furthermore, sequencing of a 2343.6 *m/z* fragment revealed that C60 was oxidized to a sulfinic acid, which complies with the assumption

that over-oxidation of C_P is the reason for the fast inactivation of this mutant under oxidizing conditions (Fig. 8). When reacted with the TrxB mutant C34S, pre-oxidized *Mt*TPx C93S yielded a hybrid peptide that unexpectedly had C80 linked to TrxB, but also a fragment indicative of the expected TPx C60 to TrxB C31 bond. Unfortunately, this fragment resisted sequencing and is isobaric with the possible peptic TrxB fragment 42–69. Over-oxidation of C60 was as evident as in the analogous experiment with wt-TrxB (Table 1, *iii*). Changing the sequence of substrate additions, i. e. adding TrxB C34S before H_2O_2, (Table 1, *iv*) prevented the over-oxidation of the C_P. The fragment indicating the reaction of TrxB with C80 of the TPx was no longer seen, which supports the assumption that the latter is an artefact resulting from a reaction with an oxidatively altered enzyme. The "correct", though ambiguous fragment indicating the TPx C60 – TrxB C31 bond, remained detectable.

Analogous experiments were then carried out with wt-*Mt*TPx (Table 1, *v* and *vi*). Irrespective of the sequence of substrate additions, a disulfide pattern identical to that obtained by oxidation of wt-TPx without any reductant (Table 1, *i*) was surprisingly observed, indicating that the formation of disulfide bonds within the wt-TPx is faster than the reduction of the sulfenic acid form by the pseudo-substrate TrxB C34S. When the pseudo-substrate, was however incubated with the oxidized enzyme over night (instead of 3 min only), the 2987.4 *m/z* fragment suggesting the formation of the TPx C60 – TrxB C31 bond was again detected (Table 1, *vii*). Because of the ambiguity of this fragment, a sample prepared identically was digested with trypsin (Table 1, *viii*). From the digest a fragment (*m/z* 5509) was isolated that was proven to represent the tryptic TPx peptide 46–65 linked to the TrxB peptide 5–35 by MS/MS sequencing (Fig. 9). Similarly, wt-*Mt*TPx, which had been pre-oxidized with 1 mM *t*-butyl hydroperoxide and then exposed to TrxC C40S overnight, yielded a tryptic fragment composed of the same TPx peptide (46–65) and the TrxC peptide 12–41. As anticipated, a variety of additional disulfide-linked fragments could be identified in the tryptic digests (not shown). The unavoidable thiol/disulfide reshuffling during tryptic digestion precludes deciding between disulfide bonds preformed between the native proteins and those generated during sample work-up. Despite extensive search, however, not a single fragment could be detected that had the exposed cysteines of the Trxs bound to C93 of *Mt*TPx, and it may be rated as highly unlikely that particularly such disulfides are completely transformed into the detected ones. It is therefore concluded that the disulfide bridges between *Mt*TrxB C31 or *Mt*TrxC C37 to C60 of *Mt*TPx, which are preferentially seen, indeed reflect the natural attack of the thioredoxins on the peroxidase.

DISCUSSION

The results presented reveal that the catalytic mechanism of atypical 2-C-peroxiredoxins, as proposed for *Ec*TPx by Choi *et al.* (9), must not be generalized, although many structural and functional parameters of this subfamily of peroxiredoxins appear to be identical. In fact, *Mt*TPx shares with *Ec*TPx (and other Prxs) a peroxidatic cysteine C_P that is activated by an arginine and a threonine; like *Ec*TPx, *Mt*TPx is a homodimer but is functionally monomeric (7,16). The resolving cysteine C95 of *Ec*TPx is conserved in homologous position of the C-terminal domain (C93 in *Mt*TPx); like *Ec*TPx (9,10) *Mt*TPx can form a disulfide bridge between the C_P and this conserved cysteine within the same subunit; in both enzymes replacement of the distal cysteine (C93 or C95, respectively) by serine was shown to affect activity, if measured with excess hydroperoxide at conventional timeframes (Fig. 1 and 10).These similarities have led to the assumptions that in the atypical 2-C-Prxs the cysteine conserved in the N-terminal domain near position 60 is C_P, which we confirm, and that the distal cysteine is generally the functional equivalent of the resolving cysteine C_R of the typical 2-C-Prxs (9,10), which is incompatible with our findings. Our stopped-flow kinetics demonstrate that in *Mt*TPx the presumed C_R is dispensable for catalysis: Neither the rate of oxidation of *Mt*TPx nor the reduction by its natural Trx substrates is significantly affected by mutating C93 to serine. In functional terms, therefore, *Mt*TPx has to be rated as a 1-C-Prx with C60 being the peroxidatic and the resolving cysteine, and the functional role of its C93 has to be redefined.

An attack by the reducing substrate(s) on the sulfenic acid form of C_P could not be directly demonstrated by LC-MS/MS analysis of reaction products of the TPx with the pseudo-substrates

*Mt*TrxB C34S and TrxC C40S, since the latter are evidently not reactive enough to compete with disulfide formation or over-oxidation of the peroxidase. When *Mt*TPx, however, was long-term exposed to the pseudo-substrates under oxidizing conditions, the latter became bound to *Mt*TPx C60 and not to C93. While the kinetic experiments convincingly demonstrate that the Trxs directly attack C_P, the MS data on pseudo-substrates adducts show that, unlike in 2-C-Prxs, the C_P remains the site of preferred attack also after formation of the disulfide form.

It should be noted that a specific C_R is only exceptionally required to complete the catalytic cycle of a peroxidase working with chalcogen catalysis. In the analogous mechanism of glutathione peroxidases oxidation and reduction takes place at the same (seleno)cysteine (22); the identical situation is postulated for 1-C-Prxs; and even typical 2-C-Prxs with a mutated C_R can catalyse the entire cycle with low molecular weight reductants such as DTT. A C_R proved to be essential only, because a direct approach of the natural proteinacious reductants to C_P is sterically hindered in the 2-C-Prxs investigated. Instead, the sulphur of C_R becomes accessible due to conformational changes during formation of a disulfide bridge between the C_P and C_R (24,25, reviewed by 14,15). In *Mt*TPx, the initially oxidized C_P, i.e. its sulfenic acid form, is evidently accessible to its natural reductants, and even in the C60–C93 disulfide form the sulphur of C60 remains similarly accessible, whereas that of C93 is not.

Being dispensable for catalysis, C93 nevertheless appears to have a pivotal role, i. e. protecting *Mt*TPx against oxidative inactivation. With exposure to hydroperoxides, *Mt*TPx C93S looses activity within seconds, and the analogous mutant of *Ec*TPx was also reported to be rapidly inactivated by oxidants (10). Furthermore, the MS data (Table 1), although qualitative only, suggests that *Mt*TPx C93S is more readily oxidized to the sulfinic acid form than the wt-enzyme. The substrate-induced inactivation reflects the tendency of enzymes working with sulphur or selenium catalysis to become inactivated if their catalytic thiol or selenol groups become oxidized to an oxidation state $\geq +4$ (26) which is a persistent hazard, if the primary oxidation products, i.e. the sulfenic or selenenic acids, are further exposed to hydroperoxides at limiting concentrations of reducing thiols. This inactivation mechanism is common in the chalcogen catalysis of the Prx (12) and GPx families (27) and could here be directly demonstrated to occur in *Mt*TPx, in particular in *Mt*TPx C93S, by mass spectroscopy. Up to the sulfinic or seleninic acid status, such over-oxidation is slowly reversed by thiols (28), but reduction of proteinacious SO_2H residues can also be accelerated by an ATP-dependent enzyme, sulfiredoxin (29), which however has not yet been detected in bacteria.

The more readily reversed oxidation level of Prxs is the disulfide status, which in the typical 2-C-Prxs is a regular catalytic intermediate. In the case of *Mt*TPx, this redox status is not an obligatory intermediate of the catalysis, but is observed, instead of the sulfenic acid form, in the absence of any reducing substrate. In this context, not only C93 but also C80 of *Mt*TPx has to be considered as reaction partner of oxidized C60, but the C60–C93 bond appears to be functionally more important, since C80 can not substitute for C93 in the protection of the enzyme against oxidative inactivation. The disulfide form may be viewed as an "alternate catalytic intermediate", which can also be reduced by thioredoxins B and C. Pertinent rate constants are evidently high, but should be distinct from those of the "regular" sulfenic acid intermediate, which explains the discrete differences of kinetic results depending on whether the analysis is started with reduced or oxidized enzyme. Unfortunately, the precise molarities of the oxidized enzyme forms remain unknown, since the mass spectroscopic analyses do not provide quantitative data. Accordingly, the kinetic experiments shown in Fig. 5 can not differentiate between reduction of the C60–C93 and C60–C80 disulfide bonds. Also, the apparent rate constants estimated for the Trx-dependent reduction of the pre-oxidized peroxidase are certainly compromised by the presence of sulfinic acid forms, which are not readily reduced in the timeframe of the experiments, or other oxidatively denatured enzyme species. Rate constants obtained for oxidized enzyme (Fig. 5) must therefore be rated as minimum estimates. Numerically, they are only lower by a factor of 5 than those obtained by steady-state kinetics (7) or stopped-flow approaches in the presence of sufficient reducing substrate (Fig. 4) and very similar for oxidized wt-*Mt*TPx and *Mt*TPx C93S (Fig. 5).

In conclusion, *Mt*TPx, when oxidized with peroxynitrite, acts as a 1-C-Prx as long as sufficient reduced Trx is available. When the reducing capacity is transiently exhausted, the peroxidatic C60 can form a disulfide bridge with C93 (and possibly with C80), which is also reduced fast by TrxB and TrxC. Unlike in typical 2-C-Prxs, however, formation of an internal disulfide bridge appears not to be an obligatory, but a facultative step of *Mt*TPx catalysis, and it certainly depends on the nature and concentration of substrates which of the alternate routes is preferentially taken. The more important role of this disulfide formation in *Mt*TPx is seen in the prevention of oxidation of C60 to sulfinic acid at excessive concentration of oxidants, which would lead to functionally incompetent enzymatic species that are not or slowly reactivated without the support of a sulfiredoxin.

Acknowledgments – We thank B. Hofmann and H.-J. Hecht (Department of Structural Biology, German Research Centre for Biotechnology, Braunschweig, Germany) for designing molecular models of *Mt*TPx forms. The work was supported by a grant from the Howard Hughes Medical Institute to RR.

REFERENCES

1. Flohé, L., and Brigelius-Flohé, R. (2001) in *Selenium. Its Molecular Biology and Role in Human Health* (Hatfield, D.L., ed.) pp. 157-178, Kluwer Academic Publishers, London
2. Sherman, D. R., Mdluli, K., Hickey, M. J., Arain, T. M., Morris, S. L., Barry, C. E., 3rd, and Stover, C. K. (1996) *Science* **272**(5268), 1641-1643
3. Zhang, Y., Heym, B., Allen, B., Young, D., and Cole, S. (1992) *Nature* **358**(6387), 591-593
4. Storz, G., Christman, M. F., Sies, H., and Ames, B. N. (1987) *Proc Natl Acad Sci U S A* **84**(24), 8917-8921
5. Sherman, D. R., Sabo, P. J., Hickey, M. J., Arain, T. M., Mahairas, G. G., Yuan, Y., Barry, C. E., 3rd, and Stover, C. K. (1995) *Proc Natl Acad Sci U S A* **92**(14), 6625-6629
6. Bryk, R., Lima, C. D., Erdjument-Bromage, H., Tempst, P., and Nathan, C. (2002) *Science* **295**(5557), 1073-1077
7. Jaeger, T., Budde, H., Flohé, L., Menge, U., Singh, M., Trujillo, M., and Radi, R. (2004) *Arch Biochem Biophys* **423**(1), 182-191
8. Li, S., Peterson, N. A., Kim, M. Y., Kim, C. Y., Hung, L. W., Yu, M., Lekin, T., Segelke, B. W., Lott, J. S., and Baker, E. N. (2005) *J Mol Biol* **346**(4), 1035-1046
9. Choi, J., Choi, S., Choi, J., Cha, M. K., Kim, I. H., and Shin, W. (2003) *J Biol Chem* **278**(49), 49478-49486
10. Baker, L. M., and Poole, L. B. (2003) *J Biol Chem* **278**(11), 9203-9211
11. Poole, L. B., and Ellis, H. R. (2002) *Methods Enzymol* **348**, 122-136
12. Poole, L. B. (2005) *Arch Biochem Biophys* **433**(1), 240-254
13. Flohé, L., Budde, H., Bruns, K., Castro, H., Clos, J., Hofmann, B., Kansal-Kalavar, S., Krumme, D., Menge, U., Plank-Schumacher, K., Sztajer, H., Wissing, J., Wylegalla, C., and Hecht, H. J. (2002) *Arch Biochem Biophys* **397**(2), 324-335
14. Hofmann, B., Hecht, H. J., and Flohé, L. (2002) *Biol Chem* **383**(3-4), 347-364
15. Wood, Z. A., Schröder, E., Robin Harris, J., and Poole, L. B. (2003) *Trends Biochem Sci* **28**(1), 32-40
16. Stehr, M., Hecht, H. J., Jaeger, T., Flohé, L., and Singh, M. (2006) *Acta Crystallogr D Biol Crystallogr*, in press
17. Higuchi, R., Krummel, B., and Saiki, R. K. (1988) *Nucleic Acids Res* **16**(15), 7351-7367
18. Radi, R., Beckman, J. S., Bush, K. M., and Freeman, B. A. (1991) *J Biol Chem* **266**(7), 4244-4250
19. Trujillo, M., Budde, H., Pineyro, M. D., Stehr, M., Robello, C., Flohé, L., and Radi, R. (2004) *J Biol Chem* **279**(33), 34175-34182
20. Mendes, P. (1997) *Trends Biochem Sci* **22**(9), 361-363
21. Koppenol, W. H., Moreno, J. J., Pryor, W. A., Ischiropoulos, H., and Beckman, J. S. (1992) *Chem Res Toxicol* **5**(6), 834-842

22. Mauri, P., Benazzi, L., Flohé, L., Maiorino, M., Pietta, P. G., Pilawa, S., Roveri, A., and Ursini, F. (2003) *Biol Chem* **384**(4), 575-588
23. Arner, E. S., and Holmgren, A. (2000) *Eur J Biochem* **267**(20), 6102-6109
24. Chae, H. Z., Chung, S. J., and Rhee, S. G. (1994) *J Biol Chem* **269**(44), 27670-27678
25. Budde, H., Flohé, L., Hecht, H. J., Hofmann, B., Stehr, M., Wissing, J., and Lünsdorf, H. (2003) *Biol Chem* **384**(4), 619-633
26. Jacob, C., Giles, G. I., Giles, N. M., and Sies, H. (2003) *Angew Chem Int Ed Engl* **42**(39), 4742-4758
27. Flohé, L. (1989) in *Glutathione: Chemical, Biochemical, and Medical Aspects - Part A* (Dolphin, D., Poulson, R., and Avramovic, O. eds.) pp. 643-731, John Wiley & Sons, Inc., Hoboken
28. Wood, Z. A., Poole, L. B., and Karplus, P. A. (2003) *Science* **300**(5619), 650-653
29. Rhee, S. G., Yang, K. S., Kang, S. W., Woo, H. A., and Chang, T. S. (2005) *Antioxid Redox Signal* **7**(5-6), 619-626

FOOTNOTES

[1]Abbreviations used: Ahp, alkyl hydroperoxidase; DHR, dihydrorhodamine; DTPA, diethylenetriamine-pentaacetic acid; DTT, dithiothreitol; *Ec*, *Escherichia coli*; INH, isoniazid; KatG, catalase/peroxidase; *Mt*, *Mycobacterium tuberculosis*; pdb, protein data bank; Prx, peroxiredoxin; RT, room temperature; SIN-1, 3-Morpholinosydnonimine hydrochloride; t-bOOH, *tert*-butyl hydroperoxide; TPx, thioredoxin peroxidase; Trx, thioredoxin; wt, wild-type

[2]The introduced starting methionine was counted as 1, which is necessary for protein expression in *E. coli*. Accordingly, C34 is equivalent to C33 in natural *Mt*TrxB.

FIGURE LEGENDS

Fig. 1: 3-Dimensional structure of *Mt*TPx. A, Ribbon representation of *Mt*TPx in its reduced state. The model was generated from the *Mt*TPx C60S variant (pdb-id 1Y25) where the serine residue was mutated back to cysteine using the Swiss-Pdb Viewer program. B, Ribbon representation of *Mt*TPx in its oxidized form (pdb-id 1XVQ). In 1XVQ C80 is oxidized and lacks the side chain probably due to radiation damage. Distance between cysteine-sulphur atoms is displayed as black lines (Ångström). Figures were produced using the program 3D-Mol from the Vector NTI-Advance software (Invitrogen Corp.).

Fig. 2: Activity determination of *Mt*TPx and molecular mutants. Substrate turnover by *Mt*TPx and molecular mutants was monitored continuously by NADPH consumption in a coupled test system at 25 °C and pH 7.4 with *t*-butyl hydroperoxide as substrate and *Mt*TrxC as cosubstrate essentially as described previously (7). Upon addition of t-bOOH (arrows; sudden drop of absorbance due to dilution) the decline in absorbance caused by wt-*Mt*TPx (D) and *Mt*TPx C80S (C) is identical, proving full activity of the latter. *Mt*TPx C60S (A) is completely inactive, while *Mt*TPx C93S (B) adopts an interim position. For the first 20 s after reaction start activity is clearly detected, while thereafter the rate of substrate turnover becomes indistinguishable from that of the inactive variant MtTPx C60S.

Fig. 3: Stopped-flow analysis of peroxynitite reduction by *Mt*TPx and molecular mutants. Peroxynitrite (18 μM) in diluted sodium hydroxide was mixed with sodium phosphate buffer pH 7 plus 0.1 mM DTPA alone (black), or plus reduced wild type *Mt*TPx (40 μM) (red), *Mt*TPx C60S (46 μM)(blue), *Mt*TPx C80S (50 μM) (green) or *Mt*TPx C93S (46 μM) (magenta) in the same buffer at 25 ºC. Final pH was 7.4.

Fig. 4: Trx-enhanced peroxynitrite reduction by *Mt*TPx and molecular mutants. A, experimental traces obtained when peroxynitrite (5.5 μM) in diluted NaOH was mixed with (a) sodium phosphate buffer 100 mM plus 0.1 mM DTPA pH 7 alone (black), (b) reduced *Mt*TPx (1.1 μM) (green), (c) reduced *Mt*TrxC (33 μM) (red) or (d) reduced MtTrxC (33 μM) plus MtTPx (1.1 μM) (blue). B, computer-assisted

simulation traces obtained for the same conditions as in A according to equations 1-4 under results. C, peroxynitrite (5.5 μM) was mixed with (a) sodium phosphate buffer 100 mM pH 7 plus 0.1 mM DTPA alone (black), (b) reduced *Mt*TrxC (33 μM) (red), (c) reduced *Mt*TrxC (33 μM) plus wild type *Mt*TPx (1.1 μM) (blue), (d) reduced *Mt*TrxC (33 μM) plus *Mt*TPx C60S (1.1 μM) (sky blue) or (e) reduced *Mt*TrxC (33 μM) plus *Mt*TPx C93S (1.1 μM) (green). D, peroxynitrite (5.5 μM) decomposition was followed (a) in sodium phosphate buffer 100 mM pH 7.4 plus 0.1 mM DTPA (black) without any further addition, (b) plus 44 μM reduced *Mt*TrxB (red), (c) and plus 44 μM reduced *Mt*TrxB and 1 μM *Mt*TPx C93S (blue). Final pH was always 7.4 ± 0.05 and the temperature was set to 25 ºC.

Fig. 5: Oxidation of *Mt*TrxB by pre-oxidized *Mt*TPx and molecular mutants. Trx oxidation was directly monitored fluorometrically at $\lambda > 335$ nm (exitation at $\lambda = 280$ nm). A, oxidation of pre-reduced *Mt*Trx B (2.25 μM) was measured (a) in sodium phosphate buffer 100 mM plus 0.1 mM DTPA pH 7.4, 25 ºC without any further addition, (black) (b) or in the presence of 22.5 μM wt-*Mt*TPx (red). The inset shows the effect of increasing wt-*Mt*TPx concentrations on the observed rate constant (k_{obs}) of *Mt*TrxB oxidation. B, oxidation of pre-reduced *Mt*TrxB (2.25 μM) in sodium phosphate buffer 100 mM plus 0.1 mM DTPA pH 7.4 25 ºC (a) plus 22.5 μM *Mt*TPx C60S (black) or plus 22.5 μM *Mt*TPx C93S (red).

Fig. 6: Prevention of peroxynitrite-dependent dihydrorhodamine oxidation by *Mt*TPx and molecular mutants. DHR (120 μM) was exposed to SIN-1 (50 μM) in sodium phosphate buffer 100 mM pH 7.4 and 25 ºC plus 0.1 mM dtpa (a) without any further addition (black) or in the presence of (b) reduced *Mt*Trx B (6.7 μM) (blue), (c) both reduced *Mt*TrxB (6.7 μM) and wt- *Mt*TPx (1.3 μM) (red), (d) both reduced *Mt*TrxB (6.7 μM) and *Mt*TPx C93S (1.3 μM) (green), (e) wt-*Mt*TPx (1.3 μM) (sky blue) and (f) oxidized *Mt*Trx B (6.7 μM) plus *Mt*TPx C93S (1.3 μM) (magenta).

Fig.7: LC-ESI-MS/MS analysis of disulfide-linked peptides obtained from peptic digestion of oxidized wt-*Mt*TPx. A, Multicharge MS spectrum of a 3261.7 *m/z* fragment, which was isolated from the peptic digest of re-oxidized *Mt*TPx. Assigned three- to six-fold charged molecular ions $[(M + 3–6\ H)^{3–6+}]$ are depicted in green. B, MS/MS spectrum of the *m/z* 816.2 ion $(M + 4\ H^+)^{4+}$. This fragment contained the sequence of *Mt*TPx 53–63 and *Mt*TPx 90–109 with confirmed partial sequences shown in red and blue, respectively.

Fig. 8: Identification of over-oxidized C60 in *Mt*TPx C93S by MS/MS sequencing. *Mt*TPx C93S was oxidized with H_2O_2 and then reacted with excess wt-*Mt*TrxB. MS/MS sequencing of TPx 49–69 fragment (parent ion m/z 1172.2^{2+}) revealed that C60 was oxidized to a sulfinic acid. The confirmed amino acid sequence of the fragment containing the over-oxidized C60 is shown in red.

Fig. 9: MS/MS sequence documentation of tryptic fragment with disulfide bridge between *Mt*TrxB C31 and *Mt*TPx C60. Wt-*Mt*TPx was oxidized with H_2O_2 and then reacted with excess *Mt*TrxB C34S over night. MS/MS (parent ion *m/z* 1378.1^{4+}) sequencing showed, that it represents the TPx peptide 46–65 linked to the TrxB peptide 5–35 with confirmed partial sequences shown in green and magenta, respectively.

TABLES

Table 1: Compilation of relevant LC-MS/MS results

	Diagnostic fragments	Molecular ion *(m/z)*	Comments
i) wt-TPx + H_2O_2 Pepsin fragmentation	wt-TPx (49–66) → (80–99) or wt-TPx (49–66) → (90–109)	4105.7	Isobaric; no sequence. Indicates disulfide bond between C60 and C80 and/or C60 and C93.
	wt-TPx (53–63) → (90–109)	3261.7	Verified by sequence; proves C60 to C93 bond (Fig. 7).
ii) TPx C93S + H_2O_2 + wt-TrxB Pepsin fragmentation	TPx C93S (49–69)	2343.6	C60 as sulfinic acid (Fig. 8); no disulfide-linked fragment detectable.
	wt-TrxB (24–41) wt-TrxB (27–41) wt-TrxB (28–41) wt-TrxB (30–41) wt-TrxB (31–41) wt-TrxB (27–38)	2076.3 1698.9 1512.7 1354.5 1168.3 1353.5	All oxidized; proves enzymatic activity of TPx C93S.
iii) TPx C93S + H_2O_2 + TrxB C34S Pepsin fragmentation	TPx C93S (49–69)	2343.6	C60 as sulfinic acid.
	TPx C93S (80–99 or 90–109) → TrxB (27–41)	3583.4	Indicates disulfide bond of TrxB to TPx C80.
	TPx C93S (49–60) → TrxB (27–41)	2987.4	Suggests disulfide bond of TrxB to TPx C60, but fragment could not be sequenced and is isobaric with TrxB (42–69).
iv) TPx C93S + TrxB + H_2O_2 Pepsin fragmentation	TPx C93S (49–60) → TrxB (27–41) only	2987.4	Suggests disulfide bond of TrxB to TPx C60. No sulfinic acid detected.
v) wt-TPx + H_2O_2 + TrxB C34S Pepsin fragmentation	Same as *i)*		Indicates slow reaction of TrxB mutant.
vi) wt-TPx + TrxB C34S + H_2O_2 Pepsin fragmentation	Same as *i)*		Indicates slow reaction of TrxB mutant.
vii) wt-TPx + TrxB C34S + H_2O_2 over night Pepsin fragmentation	wt-TPx (49–60) → TrxB (27–41)	2987.4	Suggests disulfide bond of TrxB to TPx C60.
viii) wt-TPx + TrxB C34S + H_2O_2 over night Trypsin fragmentation	wt-TPx (46–65) → TrxB (5–35)	5509	Verified by sequence (Fig. 9); proves disulfide bond between C31 of TrxB and C60 of TPx.
ix) wt-TPx + *t*-bOOH + TrxC C40S over night Trypsin fragmentation	wt-TPx (46–65) → TrxC (12–41)	5348	Proves disulfide bond between C37 of TrxC and C60 of TPx.

FIGURES

Fig. 1

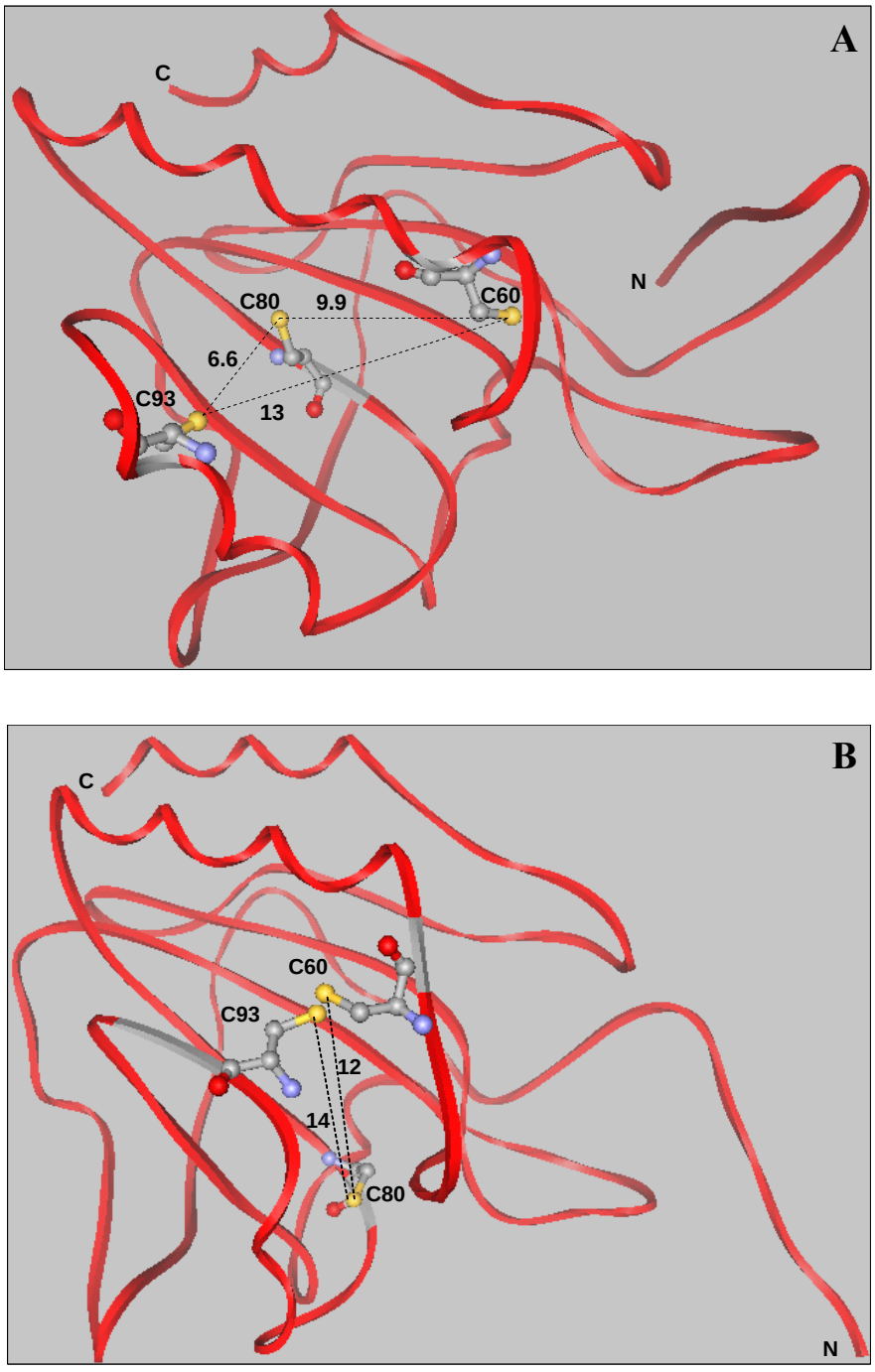

Fig. 2

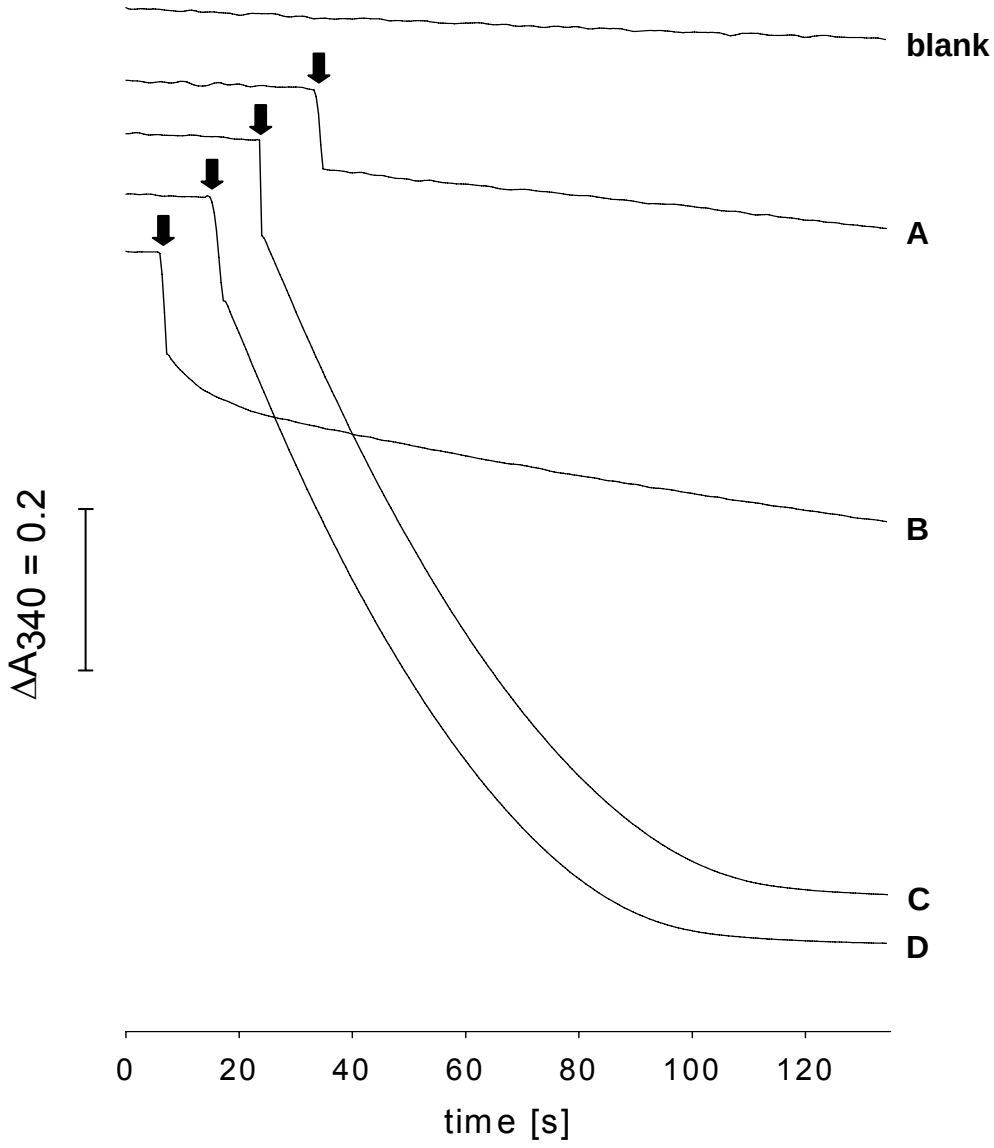

Fig. 3

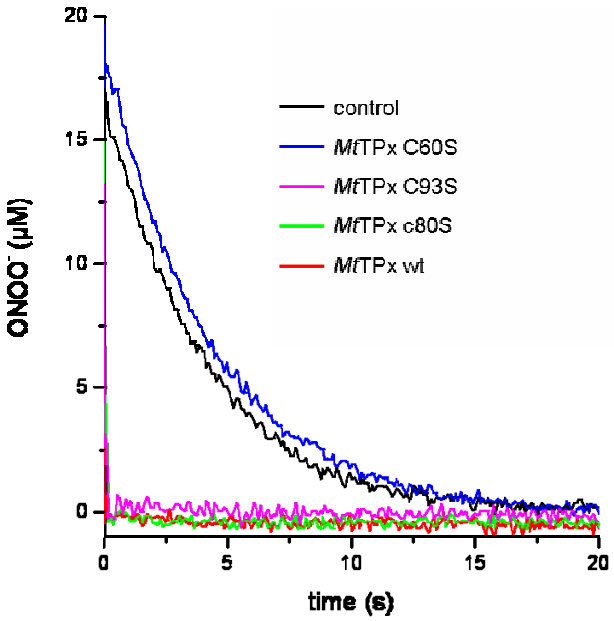
20
15
10
5
0
0
5
10
15
20
ONOO⁻ (μM)
time (s)
control
MtTPx C60S
MtTPx C93S
MtTPx c60S
MtTPx wt

Fig. 4

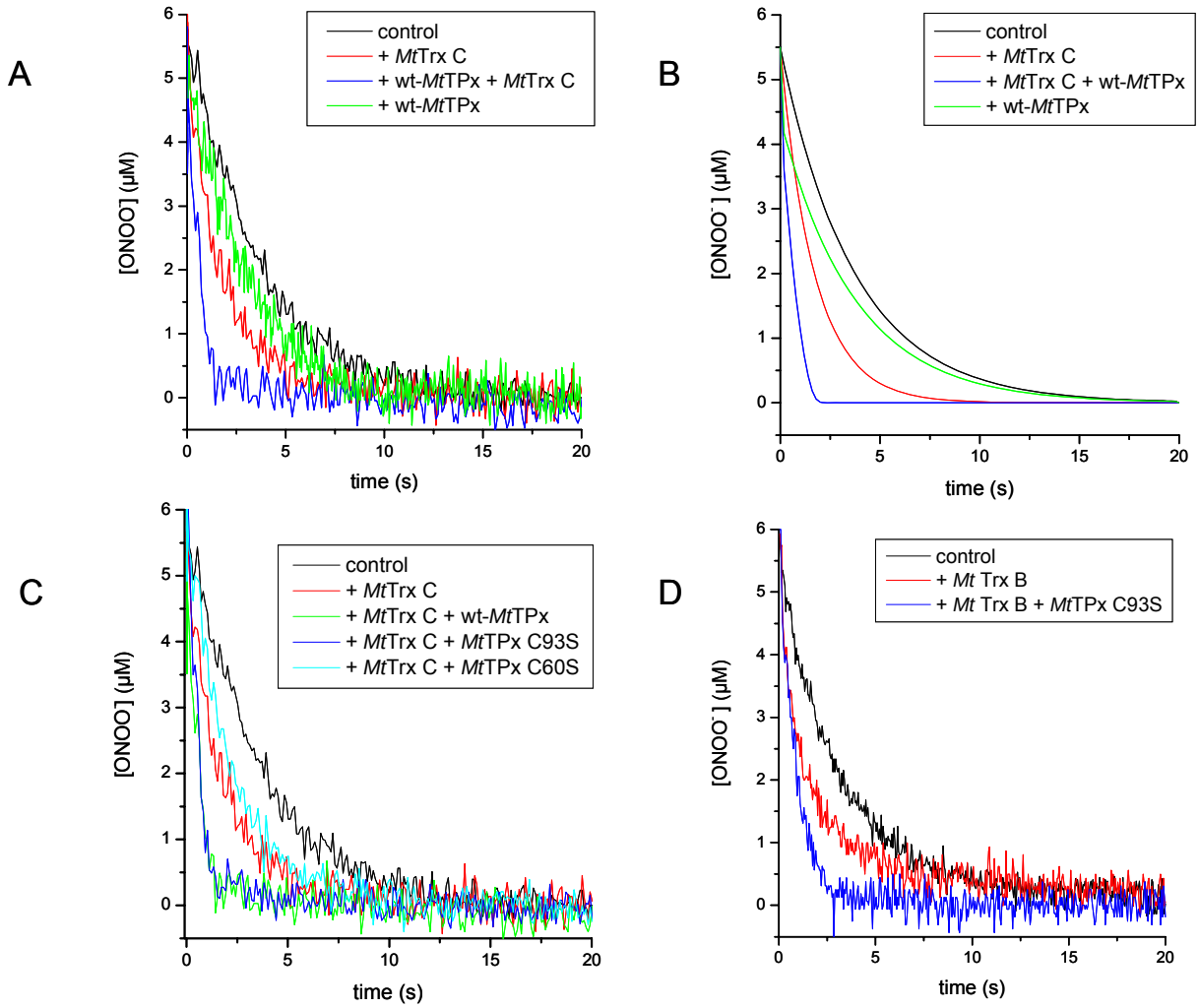
A
control
+ MtTrx C
+ wt-MtTPx + MtTrx C
+ wt-MtTPx
[ONOO] (μM)
time (s)
B
control
+ MtTrx C
+ MtTrx C + wt-MtTPx
+ wt-MtTPx
[ONOO-] (μM)
time (s)
C
control
+ MtTrx C
+ MtTrx C + wt-MtTPx
+ MtTrx C + MtTPx C93S
+ MtTrx C + MtTPx C60S
[ONOO] (μM)
time (s)
D
control
+ Mt Trx B
+ Mt Trx B + MtTPx C93S
[ONOO-] (μM)
time (s)

Fig. 5

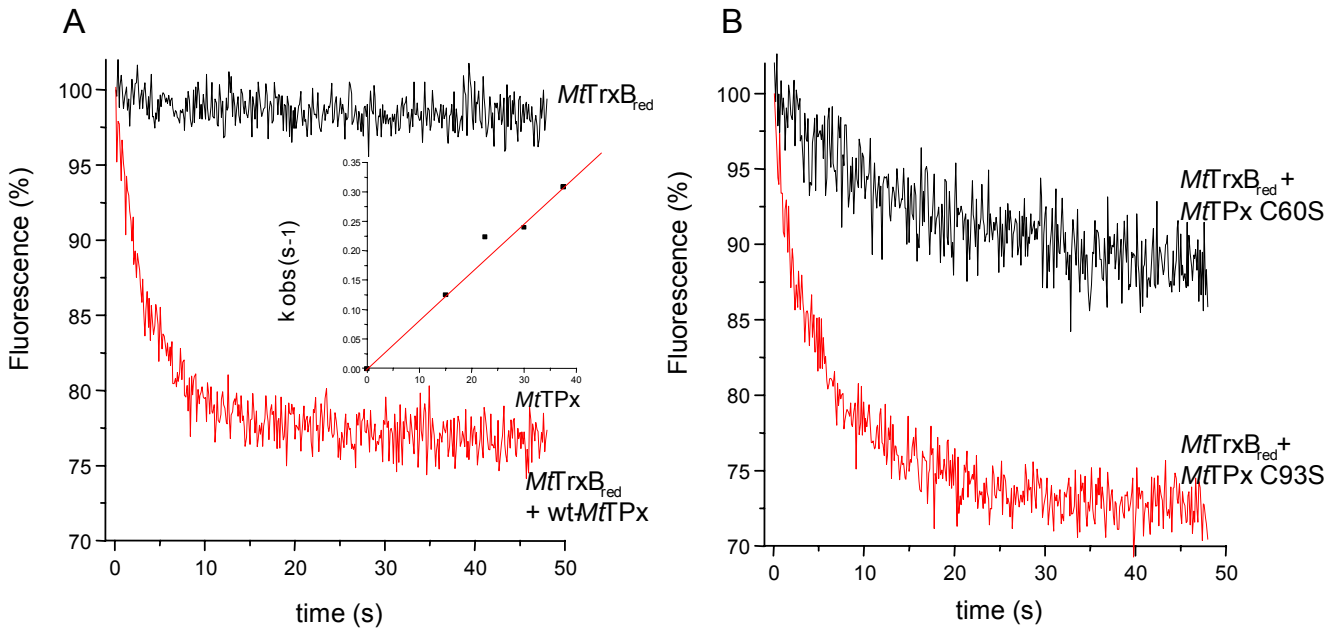
A
B
Fluorescence (%)
time (s)
MtTrxB red
MtTrxB red + wt-MtTPx
k obs (s-1)
MtTPx
MtTrxB red + MtTPx C60S
MtTrxB red + MtTPx C93S

Fig. 6

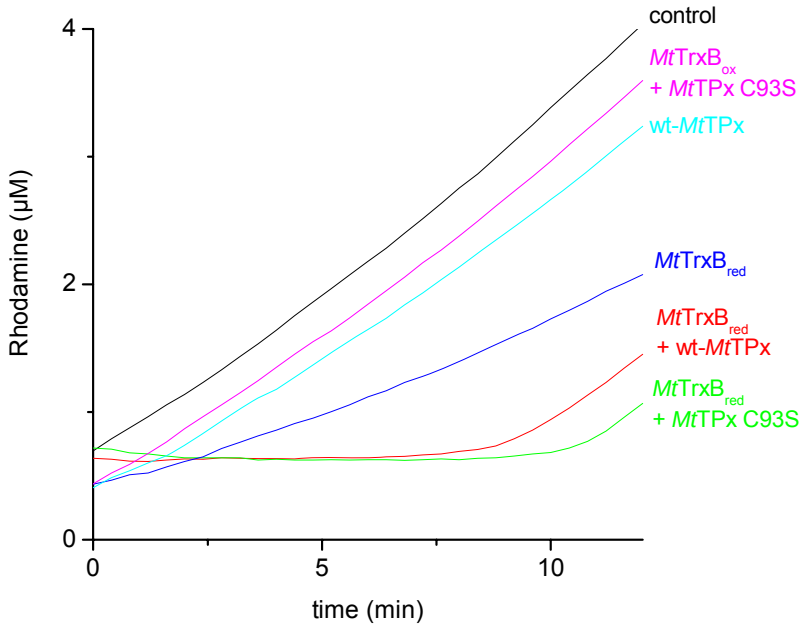
control
MtTrxB ox
+ MtTPx C93S
wt-MtTPx
MtTrxB red
MtTrxB red
+ wt-MtTPx
MtTrxB red
+ MtTPx C93S
Rhodamine (µM)
time (min)
0
2
4
0
5
10

Fig. 7

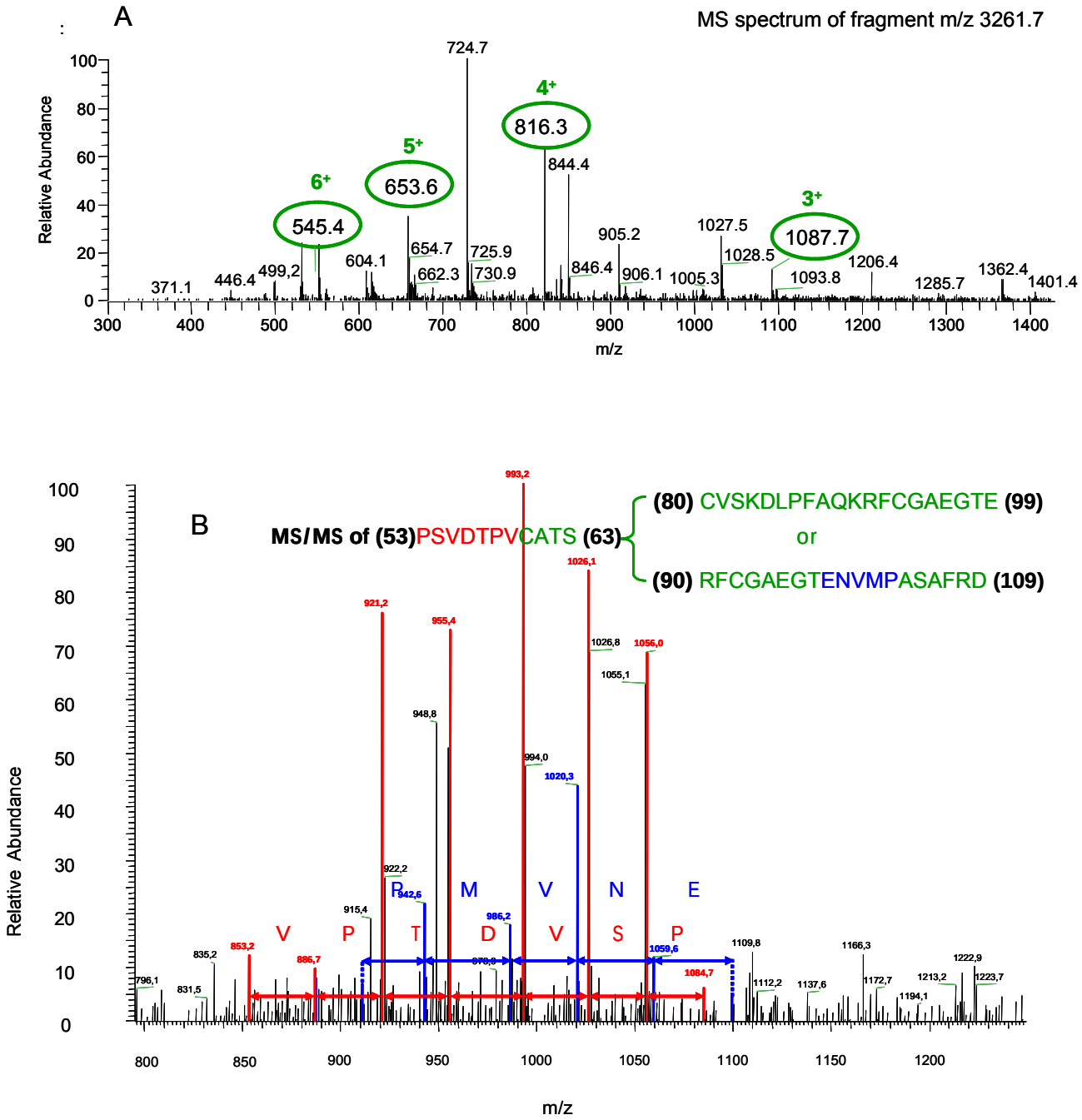
A
MS spectrum of fragment m/z 3261.7
Relative Abundance
m/z
6+
545.4
5+
653.6
4+
816.3
3+
1087.7
724.7
844.4
905.2
1027.5
371.1
446.4
499.2
604.1
654.7
662.3
725.9
730.9
846.4
906.1
1005.3
1028.5
1093.8
1206.4
1285.7
1362.4
1401.4
B
MS/MS of (53)PSVDTPVCATS (63)
(80) CVSKDLPFAQKRFCGAEGTE (99)
or
(90) RFCGAEGTENVMPASAFRD (109)
Relative Abundance
m/z
V P T D V S P
P M V N E

Fig. 8

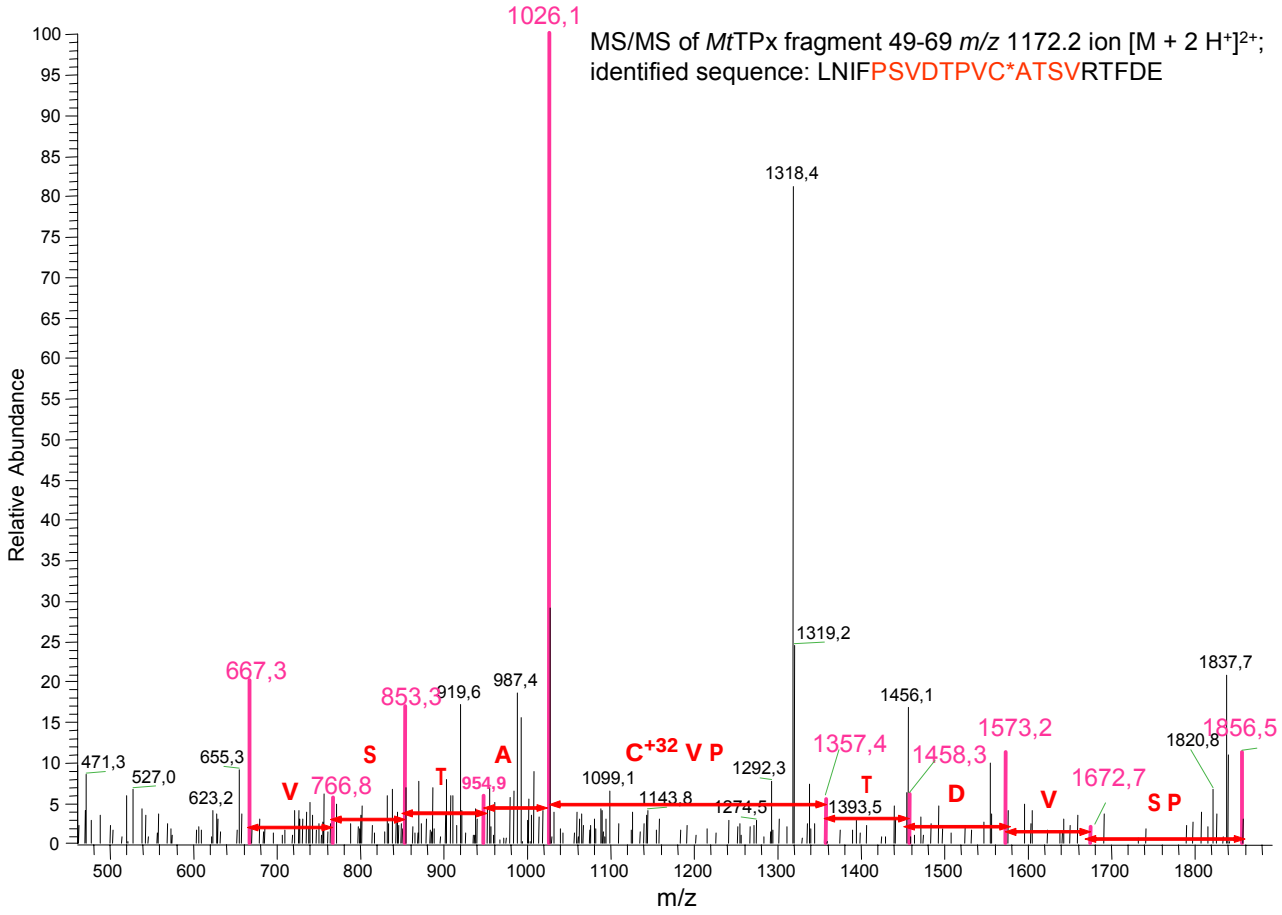
MS/MS of *Mt*TPx fragment 49-69 *m/z* 1172.2 ion [M + 2 H+]2+;
identified sequence: LNIFPSVDTPVC*ATSVRTFDE
Relative Abundance
m/z
1026,1
1318,4
1319,2
667,3
853,3
919,6
987,4
1837,7
1456,1
1573,2
1856,5
1820,8
1357,4
1458,3
1672,7
471,3
527,0
655,3
623,2
766,8
954,9
1099,1
1143,8
1274,5
1292,3
1393,5
V
S
T
A
C+32 V P
T
D
V
S P

Fig. 9

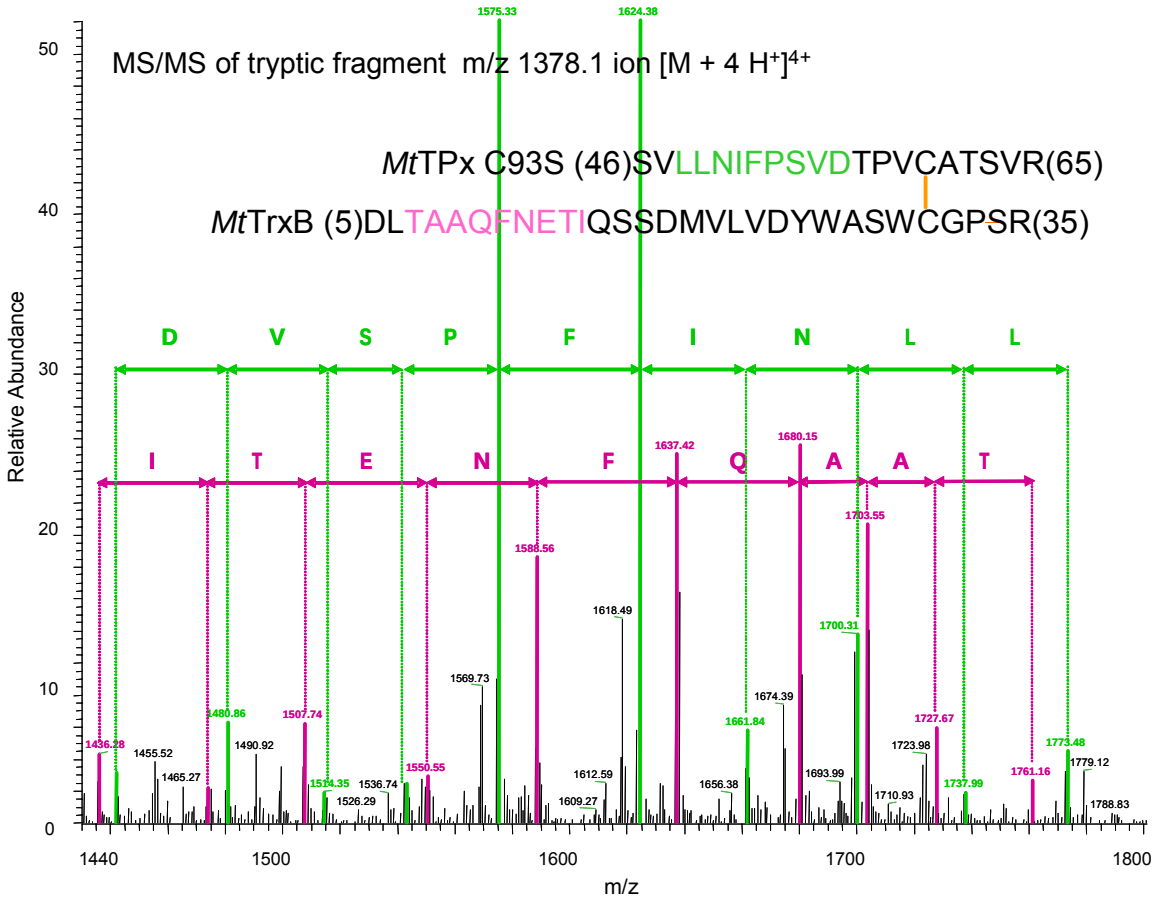
MS/MS of tryptic fragment m/z 1378.1 ion [M + 4 H+]4+
MtTPx C93S (46)SVLLNIFPSVDTPVCATSVR(65)
MtTrxB (5)DLTAAQFNETIQSSDMVLVDYWASWCGPSR(35)
D V S P F I N L L
I T E N F Q A A T
Relative Abundance
m/z
0
10
20
30
40
50
1440
1500
1600
1700
1800
1575.33
1624.38
1637.42
1680.15
1703.55
1588.56
1618.49
1700.31
1569.73
1674.39
1661.84
1727.67
1773.48
1779.12
1723.98
1737.99
1761.16
1788.83
1710.93
1693.99
1656.38
1612.59
1609.27
1480.86
1507.74
1490.92
1436.28
1455.52
1465.27
1514.35
1536.74
1526.29
1550.55